Quantum Storage of Frequency-Multiplexed Heralded Single Photons

Alessandro Seri,[1,*,†] Dario Lago-Rivera,[1,*] Andreas Lenhard,[1] Giacomo Corrielli,[2] Roberto Osellame,[2] Margherita Mazzera,[1] and Hugues de Riedmatten[1,3]

[1]*ICFO-Institut de Ciencies Fotoniques, The Barcelona Institute of Technology, Mediterranean Technology Park, 08860 Castelldefels (Barcelona), Spain*

[2]*Istituto di Fotonica e Nanotecnologie (IFN)—CNR and Dipartimento di Fisica—Politecnico di Milano, P.zza Leonardo da Vinci 32, 20133 Milano, Italy*

[3]*ICREA-Institució Catalana de Recerca i Estudis Avançats, 08015 Barcelona, Spain*

(Received 20 December 2018; revised manuscript received 29 March 2019; published 22 August 2019)

We report on the quantum storage of a heralded frequency-multiplexed single photon in an integrated laser-written rare-earth doped waveguide. The single photon contains 15 discrete frequency modes separated by 261 MHz and spanning across 4 GHz. It is obtained from a nondegenerate photon pair created via cavity-enhanced spontaneous down-conversion, where the heralding photon is at telecom wavelength and the heralded photon is at 606 nm. The frequency-multimode photon is stored in a praseodymium-doped waveguide using the atomic frequency comb (AFC) scheme, by creating multiple combs within the inhomogeneous broadening of the crystal. Thanks to the intrinsic temporal multimodality of the AFC scheme, each spectral bin includes 9 temporal modes, such that the total number of stored modes is about 130. We demonstrate that the storage preserves the nonclassical properties of the single photon, and its normalized frequency spectrum.

DOI: 10.1103/PhysRevLett.123.080502

Quantum memories for light are important devices in quantum information science [1,2]. Important progress has been reported in recent years, e.g., in terms of storage time [3–5], storage and retrieval efficiency [6–9] and storage bandwidth [10,11]. Multimode quantum memories would greatly help the scaling of quantum networks by decreasing the entanglement distribution time between remote quantum nodes [1,12]. Current research focuses mostly on time multiplexing in rare-earth doped crystals [13–22] and in spatial multiplexing in atomic gases [23–28]. Beyond these demonstrations, rare-earth doped crystals, thanks to their large inhomogeneous broadening, represent a unique quantum system which could also add another degree of freedom for multiplexing, i.e., the storage of multiple frequency modes [29]. This unique ability could also enable the generation of high-dimensional frequency entanglement between a photon and a matter system. Furthermore, it could also provide a quantum memory for frequency bin-encoded qubits, which are gaining interest both in quantum information and computation [30–34]. Here, we report on the first demonstration of quantum storage of a frequency-multiplexed single photon into a laser-written waveguide integrated in a $Pr^{3+}:Y_2SiO_5$ crystal. The multimode capability of our memory is further increased thanks to the intrinsic temporal multimodality of the storage protocol used, i.e., the atomic frequency comb. The great advantage of using waveguides is that the power required to prepare the quantum memory is strongly reduced due to the increased light-matter interaction. This enables simultaneous preparation of several memories at different frequencies, with a moderate laser power.

Very few experiments have explored the storage of frequency-multiplexed photonic states. Qubits encoded with weak coherent states have been stored in up to 26 frequency modes in the excited state of a Tm-doped waveguide [29], and up to two modes in the spin state of a Pr-doped crystal [22]. Parts of the spectrum of a broadband single photon were also stored in up to 6 frequency bins in an Er-doped optical fiber [35]. In contrast, our source naturally generates photon pairs in discrete frequency bins [36] that can all be stored in our crystal.

In this Letter, we demonstrate the storage of a frequency-multiplexed heralded single photon, consisting of about 15 modes, in a Pr^{3+}-doped waveguide [36]. This leads to an increase of our count rates by 5.5 with respect to the single frequency mode storage that allows us to make a detailed analysis of the multiplexed biphoton state after the storage. We demonstrate the nonclassicality of the correlations of the multiplexed biphoton after a preprogrammed storage time of 3.5 μs. We also show that the normalized spectrum of our single photon is well preserved during the storage.

The setup, Fig. 1(a), consists of two main parts: the photon-pair source and the memory. The first is based on cavity-enhanced spontaneous parametric down-conversion (CSPDC) [37]. The idler photon, at 1436 nm (telecom E-band), heralds the presence of a signal photon resonant with an optical transition of Pr^{3+} at 606 nm. Around the SPDC source, a cavity resonant both with the idler and the

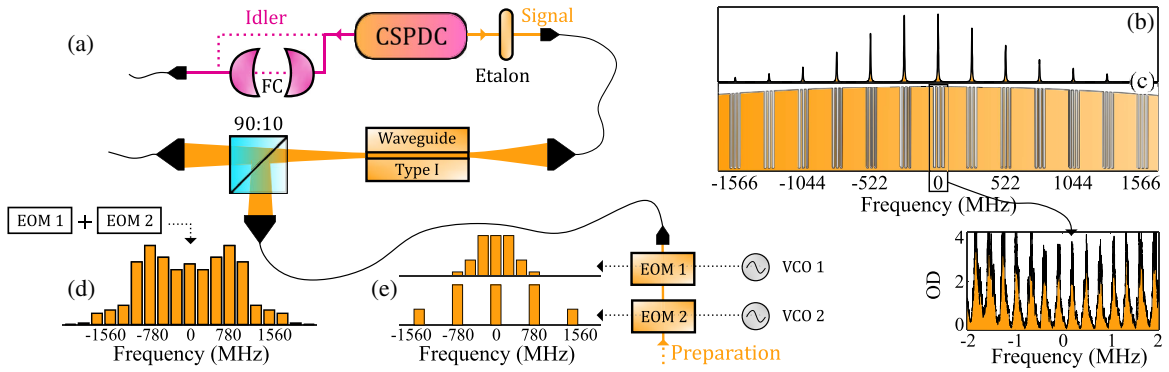

FIG. 1. (a) Experimental setup. From the photon-pair source (CSPDC) the idler photon (purple beam) is coupled to a fiber, either directly or after passing through a filter cavity (FC). The signal photon (orange beam) is sent to the memory crystal (waveguide type I). The preparation light (bottom) is modulated with two EOMs: EOM_1 (EOM_2) is driven with a voltage controlled oscillator VCO_1 @261.1 MHz (VCO_2 @3x261.1 MHz). A 90:10 (T:R) beam splitter couples 10% of the preparation beam into the waveguide, counterpropagating with the signal photons. The modulation given by each EOM is in (e), the resulting one in (d). (b) Sketch of the generated biphoton spectrum. (c) Sketch of the inhomogeneous broadening, tailored with many atomic frequency combs (AFCs). The inset is a trace of a measured AFC ($\tau = 3.5$ μs, measured internal efficiency $\eta_{\mathrm{AFC}}^{\mathrm{int}} = 8.5\%$ [39]) in optical depth (OD).

signal frequencies redistributes the biphoton spectrum along narrow frequency modes [Fig. 1(b)]. These modes are separated by the cavity free spectral range (FSR = 261.1 MHz) and have a linewidth of 1.8 MHz. Because the signal and idler photons have different FSR, only a few modes (15 in our case) are generated [38]. So far, only the central frequency mode [at frequency 0 in Fig. 1(b)] was heralded and stored [19,36]. For most of the measurements reported here, the idler photon is directly sent to a single photon detector (SPD), resulting in a frequency-multimode heralding (MMi). Occasionally, a homemade Fabry-Perot filter cavity [FC in Fig. 1(a)] is used to provide a single frequency heralding (SMi).

The signal photon, filtered with an etalon, is coupled into a SM fiber and sent to the memory optical table. We store the signal photons in a 0.05% doped $Pr^{3+}:Y_2SiO_5$ crystal at cryogenic temperature (<3 K), where a laser-written type I waveguide was fabricated by femtosecond laser micromachining [36]. If we want the photons to be transmitted through the waveguide, we produce a transparency window (spectral pit) around the signal frequency mode. The implemented storage protocol is the atomic frequency comb (AFC) technique [40,41]: in this protocol the absorption line of the crystal is tailored into a periodical absorptive structure by optical pumping [inset of Fig. 1(c)]. A photon absorbed by such structure is mapped into a collective superposition of atomic excitations. After a preprogrammed time, dependent on the comb periodicity, the atomic excitations rephase, releasing an echo of the incoming photon along the same direction. To store the whole spectrum of the frequency-multiplexed photons, we send the preparation beam to two cascaded electro-optical modulators ($EOM_{1,2}$) with resonance frequencies equal to $1 \times$ FSR and $3 \times$ FSR of the CSPDC source, respectively [see spectrum in Fig. 1(d)]. With this method, using the same preparation time that we would need to prepare just one comb, we simultaneously tailor many AFCs (up to 15 demonstrated here), all for the same τ (3.5 μs) and with the same internal efficiency ($\eta_{\mathrm{AFC}}^{\mathrm{int}} = 8.5\%$) within the inhomogeneous absorption profile of Pr^{3+} [Fig. 1(c), the inset shows a measured AFC trace]. Hence, to perform multimode storage (MMs) we switch on both EOMs, while we switch them off to store just a single mode (SMs), i.e., to prepare the AFC only at the central frequency-mode. We note that this method has a very favorable scalability, as the spectral modes stored scale exponentially with the number of EOMs used ($>3^{\#\mathrm{EOMs}}$). The total efficiency of the storage, considering the memory as a black box, is given by $\eta_{\mathrm{AFC}}^{\mathrm{int}}$ times the coupling of the photon into and out of the waveguide (40% in the present experiment) [39].

As a figure of merit for our photon pairs, we use the second-order normalized cross-correlation function between signal and idler fields, defined as $g_{s,i}^{(2)}(\Delta t) = p_{s,i}/(p_s p_i)$, where $p_{s,i}$ is the probability to detect a coincidence between the two and p_s (p_i) the probability to detect independently a signal (idler) photon in a time window Δt. We measured $g_{s,i}^{(2)}$ vs pump power (P) for the heralded photons before and after the storage [brown empty and orange full dots in Fig. 2(a), respectively]. Here, both the idler and signal photons are multimode (MMi-MMs). An example of a trace from which we extract the $g_{s,i}^{(2)}$ is shown in the inset of Fig. 2(a): the brown and orange traces represent coincidence histograms between the idler and signal photons ($P = 3$ mW) measured before the memory setup and after the storage, respectively. The time window considered, $\Delta t = 400$ ns, is shown as a darker region in both the traces. Thanks to the intrinsic temporal multimodality of the AFC scheme [41], we store 3.5 μs/400 ns ~ 9 distinguishable temporal modes.

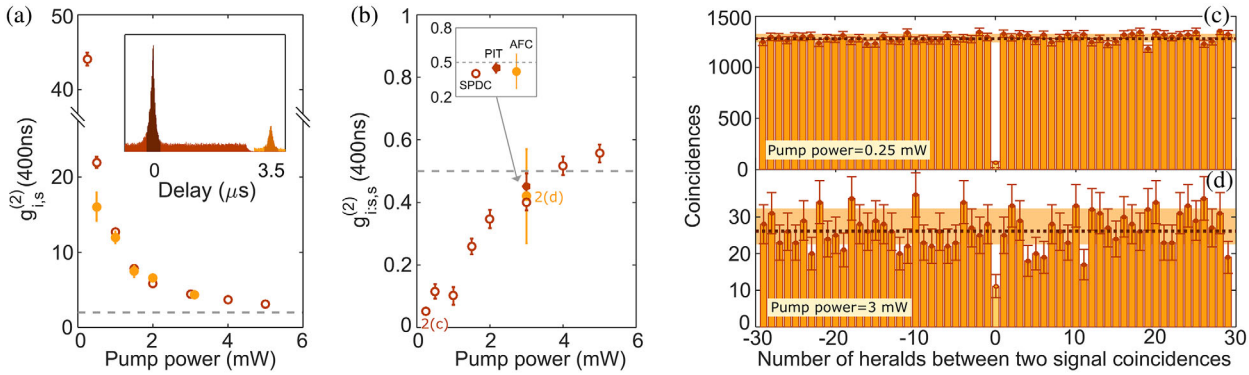

FIG. 2. (a) Second order cross-correlation value $g^{(2)}_{s,i}(\Delta t)$ vs pump power (P) for the photon-pair source alone (empty brown circles) and after the storage of the signal (plain orange points). The inset shows a temporal coincidence histogram between signal and idler photons at $P = 3$ mW (the input photon in brown and AFC echo in orange). (b) Conditional autocorrelation of the signal photon $g^{(2)}_{i:s,s}(400\text{ ns})$ vs P for the source alone (empty brown circles). $g^{(2)}_{i:s,s}(400\text{ ns})$ for the signal photon transmitted through a spectral pit (plain brown dots) or after storage (plain orange points) are also shown for $P = 3$ mW. (c) Autocorrelation histogram for the source alone for $P = 0.25$ mW. (d) Autocorrelation histogram of the stored signal photons for $P = 3$ mW (measurement time >44 h).

As expected for a two-mode squeezed state [42], the $g^{(2)}_{s,i}$ increases while decreasing P [Fig. 2(a)]. All the data points are above the classical limit (gray dotted line), defined by the Cauchy-Schwarz inequality as $\sqrt{g^{(2)}_{i,i}\, g^{(2)}_{s,s}}$ (for simplicity we overestimate a classical limit of 2). Except for the point at 0.5 mW, where the coincidence rate becomes comparable to the noise rate, the $g^{(2)}_{s,i}$ after the storage follows the same behavior of the measurement with the source only.

To fully characterize the nonclassicality of the biphoton, we measured the heralded autocorrelation of the signal photon $g^{(2)}_{i:s,s}$, namely, the autocorrelation of the signal photon conditioned on an idler detection [43]. Here again, both the heralding and the signal photons are multimode (MMi-MMs). The signal photons are split by a fiber beam splitter and detected with two SPDs. A $g^{(2)}_{i:s,s}$ histogram measured before the memory setup for $P = 0.25$ mW is reported in Fig. 2(c). The $g^{(2)}_{i:s,s}$ has been measured before the memory setup for different P, the lowest point [extracted from Fig. 2(c)] being $g^{(2)}_{i:s,s}(400\text{ ns}) = 0.052 \pm 0.007$, deep in the single photon regime. To overcome the low statistics, we repeated the measurement of the $g^{(2)}_{i:s,s}$ for $P = 3$ mW sending the signal photons to the memory setup, and preparing a multimode spectral pit or AFC. The comparison of the results for the same pump power is shown in the inset of Fig. 2(b). All the measured data points of Fig. 2(b) are below the classical limit of 1. Moreover, the $g^{(2)}_{i:s,s}$ measured at 3 mW after the spectral pit $[g^{(2)}_{i:s,s}(400\text{ ns}) = 0.45 \pm 0.04]$ or after the storage in the AFC $[g^{(2)}_{i:s,s}(400\text{ ns}) = 0.42 \pm 0.15]$ are both compatible with the measurement performed before the memory setup $[g^{(2)}_{i:s,s}(400\text{ ns}) = 0.40 \pm 0.03]$. We thus conclude that the storage in the memory does not degrade the statistics of the single photons.

We now study the spectrum of our signal photons, before and after the storage. A signature of the presence of different frequency modes is the beating between them in the temporal $g^{(2)}_{s,i}$ function [Fig. 3(a)] [44]. The expected beating has a periodicity of ~3.8 ns (1/FSR). We then recalculate the histograms with increased resolution [Fig. 3(b) before the storage, Fig. 3(c) after]. The clear beating in the AFC echo, with the inferred periodicity, is a strong signature that the storage protocol preserves the frequency multimodality of the photon. We expect the width of the oscillation peaks to decrease with the number

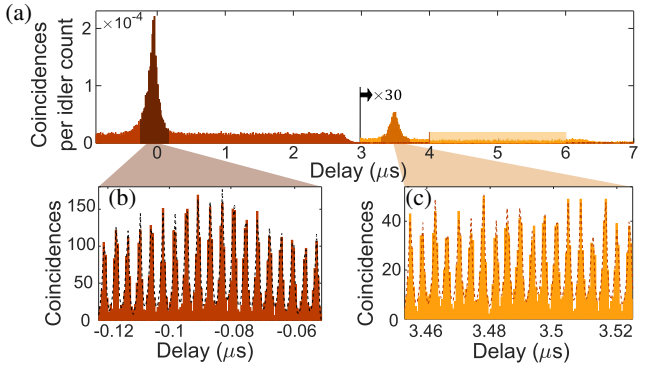

FIG. 3. (a) Temporal coincidence histogram between idler and signal photons after the source (brown) or after storage (orange). The rectangle between 4 and 6 μs is the stored noise, i.e., the accidental counts $p_s p_i$ in the $g^{(2)}_{s,i}$ of the AFC echo (the accidental counts for the input are measured before the brown peak). Panels (b) and (c) show an enlargement of the peaks, where the beating between the spectral modes is visible. The width of the beating peaks extracted from the fits is (910 ± 60) ps, comparable to the 970 ps expected [39].

of spectral modes interfering [44]; however, the time jitter of our detection system allows us only to infer a lower bound of 4 [39].

To quantify the number of generated and stored frequency modes, we send the idler photons into the FC [Fig. 1(a)] that we scan about 4 GHz, covering the whole spectrum of the idler photons. We thus herald different signal frequency modes at different times. The coincidences detected before and after the storage are plotted in Figs. 4(a) and 4(b) in brown and orange, respectively. In the SMs case, we just detect coincidences when the FC is in resonance with the stored mode [Fig. 4(a)]; if we switch on the two EOMs (MMs), we can store and retrieve the whole spectrum of the signal photon [Fig. 4(b)], i.e., about 15 spectral modes. As the spectrum of the preparation beam is almost flat for the nine central modes [Fig. 1(d)], the biggest part of the spectrum is stored with the same efficiency of the SMs case. Despite the lower preparation power, also the other modes are stored with comparable efficiencies. We quantify the similarity of the normalized spectrum of the heralded photon before and after the storage from the measurements shown in Fig. 4(b). We extract the count rate and the $g^{(2)}_{s,i}$ of each frequency mode and define an overlap function ranging from 0 (no overlap) to 1 (perfect overlap). We find an overlap between the count rates of 0.97 ± 0.03 and of 0.98 ± 0.06 between the $g^{(2)}_{s,i}$ values. More details on this analysis can be found in the Supplemental Material [39].

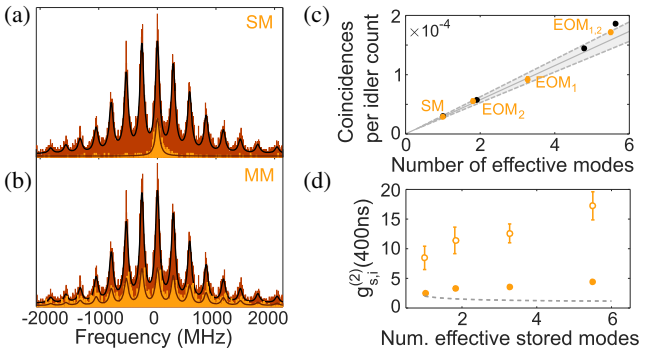

FIG. 4. (a)–(b) Heralded signal detections triggered to the scan of the FC in the case of SM and MM storage, respectively. The brown (orange) histogram is measured with the source alone (after the storage). The solid lines are fits to the brown histogram, renormalized to overlap with the orange trace. (c) Normalized coincidences between idler detections and signal photons, either after being transmitted through a spectral pit (black dots) or being stored (orange dots), vs number of effective modes N_{eM}. The gray line is fixed to pass through the origin and the first orange point ($N_{\mathrm{eM}} = 1$), the gray area being the error. The coincidence rate after the spectral pit is multiplied by the storage internal efficiency ($\eta^{\mathrm{int}}_{\mathrm{AFC}} = 8.5\%$ [39]), to compare all the results with the same line. (d) $g^{(2)}_{s,i}$ measured vs number of effective stored modes. The orange full (empty) points are measured with $P = 3$ mW (1 mW). The gray dotted line is the theoretical classical limit, which scales with the number of modes N as $1 + 1/N$ (the real bound would be lower, due to noise and a finite detection window of 400 ns) [39,45].

As the spectrum of our biphoton is not flat [Fig. 1(b)], the count rate does not increase linearly with the number of stored modes. We define an *effective mode* as a mode whose count rate is the same as the one of the central frequency mode. Hence, if we store just the central mode (SMs), we store 1 effective mode. On the other hand, the whole spectrum of the photon (15 spectral modes) will be equivalent to 5.6 effective modes. By using different EOM configurations, we can vary the number of effective modes stored (N_{eM} [39]). The light orange data points in Fig. 4(c) show the measured coincidence rate in the retrieved AFC echo vs N_{eM}. For this measurement the idler photon is not filtered (MMi). When increasing N_{eM}, the coincidence rate increases linearly, as expected. The same measurement is performed by preparing a multimode spectral pit [black dots in Fig. 4(c)]. For each EOM configuration considered in Fig. 4(c), we also measure the cross-correlation of the AFC echo [full points of Fig. 4(d)]. In this case, the $g^{(2)}_{s,i}$ increases with N_{eM} because, even if both the coincidences and the stored noise increase linearly, there is a part of uncorrelated noise (due to dark counts or broadband noise), which remains constant [39].

The multimode storage technique demonstrated in this Letter is directly suitable for storing the frequency bin entanglement naturally generated by our source [32]. For that purpose it is desirable to reach higher values of $g^{(2)}_{s,i}$. An easy way to increase the $g^{(2)}_{s,i}$ without destroying the entangled state is to reduce the pump power of the source (as shown in Fig. 2). We measure the $g^{(2)}_{s,i}$ vs N_{eM}, for $P =$ 1 mW [empty orange points in 4(d)]. Despite the fact that the coincidence rate decreases together with P, the $g^{(2)}_{s,i}$ increases remarkably with respect to the previous measurement. The $g^{(2)}_{s,i}$ would increase further by filtering broadband noise before the idler detection with an etalon.

Another possible application of frequency multimode storage is to use each spectral channel as an independent quantum memory, leading to spectral multiplexing, e.g., for quantum repeaters [29]. For this purpose we should distinguish the different heralding frequency modes, i.e., separate the modes of the idler photon [46]. This would destroy the frequency bin entanglement, but the count rate

TABLE I. Measured $g^{(2)}_{s,i}$ after storage in different configurations.

SM_s	MM_i	2.48 ± 0.17
MM_s	MM_i	4.35 ± 0.22
MM_s	SM_i	15.8 ± 1.5
SM_s	SM_i	72 ± 12

and duty cycle of the experiment would increase, without decreasing the $g^{(2)}_{s,i}$. While it is challenging to distinguish the different idler frequency modes with current technology due to their small separation, we perform a series of measurements to validate our statement. We compare the $g^{(2)}_{s,i}$ measured with a single mode (SM_i) or multimode heralding photon (MM_i), storing either one mode (SM_s) or the whole spectrum (MM_s) of the signal photon (see Table I).

We note that, distinguishing the spectral modes of the heralding detections (SM_i), the $g^{(2)}_{s,i}$ of the retrieved multimode echo would increase. Moreover, if we could retrieve independently the different modes of the signal (fourth case), the $g^{(2)}_{s,i}$ for each spectral mode would be increased by a factor of 16, without decreasing the experiment count rate. We could also perform spin-wave storage [19,47] addressing spin states for each frequency mode individually, e.g., using serrodyne frequency shifting of the control beams [48], having therefore a SM_s-SM_i configuration.

We demonstrated quantum storage of a frequency multiplexed single photon, counting 15 spectral modes over 4 GHz, in an integrated rare-earth-doped laser-written waveguide. Our work opens prospects for the realization of frequency multiplexed quantum repeaters, and for the demonstration of high dimensional frequency entanglement between light and matter. Together with the 9 temporal modes stored as an intrinsic property of the AFC protocol, we demonstrate the storage of more than 130 individual modes. Our results show that integrated waveguides in rare-earth doped crystals can be used as versatile light-matter interaction platforms with both time and frequency multiplexing capabilities. Moreover, the unique three-dimensional fabrication capability of laser-written waveguides [49] also holds promises for implementing large memory arrays in one crystal and allows fabrication of optical angular momentum compatible waveguides [50]. The ability to combine several multiplexing capabilities in one system would open the door to the realization of massively multiplexed quantum memories.

We acknowledge financial support by the European Research Council (ERC) via the Advanced Grant CAPABLE (742745), by the European Union via the Quantum Flagship project QIA (820445), by the Spanish Ministry of Economy and Competitiveness (MINECO) and Fondo Europeo de Desarrollo Regional (FEDER) (FIS2015-69535-R), by MINECO Severo Ochoa through Grant No. SEV-2015-0522, by Fundació Cellex, and by CERCA Programme/Generalitat de Catalunya.2020

*These authors contributed equally to this work.
†alessandro.seri@icfo.eu

[1] N. Sangouard, C. Simon, H. de Riedmatten, and N. Gisin, Rev. Mod. Phys. **83**, 33 (2011).
[2] M. Afzelius, N. Gisin, and H. de Riedmatten, Phys. Today **68**, No. 12, 42 (2015).
[3] A. G. Radnaev, Y. O. Dudin, R. Zhao, H. H. Jen, S. D. Jenkins, A. Kuzmich, and T. A. B. Kennedy, Nat. Phys. **6**, 894 (2010).
[4] S.-J. Yang, X.-J. Wang, X.-H. Bao, and J.-W. Pan, Nat. Photonics **10**, 381 (2016).
[5] M. Körber, O. Morin, S. Langenfeld, A. Neuzner, S. Ritter, and G. Rempe, Nat. Photonics **12**, 18 (2018).
[6] M. P. Hedges, J. J. Longdell, Y. Li, and M. J. Sellars, Nature (London) **465**, 1052 (2010).
[7] Y.-W. Cho, G. T. Campbell, J. L. Everett, J. Bernu, D. B. Higginbottom, M. T. Cao, J. Geng, N. P. Robins, P. K. Lam, and B. C. Buchler, Optica **3**, 100 (2016).
[8] P. Vernaz-Gris, K. Huang, M. Cao, A. S. Sheremet, and J. Laurat, Nat. Commun. **9**, 363 (2018).
[9] Y. Wang *et al.*, Nat. Photonics **13**, 346 (2019).
[10] K. T. Kaczmarek *et al.*, Phys. Rev. A **97**, 042316 (2018).
[11] J.-P. Dou *et al.*, Commun. Phys. **1**, 55 (2018).
[12] C. Simon, H. de Riedmatten, M. Afzelius, N. Sangouard, H. Zbinden, and N. Gisin, Phys. Rev. Lett. **98**, 190503 (2007).
[13] I. Usmani, M. Afzelius, H. de Riedmatten, and N. Gisin, Nat. Commun. **1**, 12 (2010).
[14] C. Clausen, I. Usmani, F. Bussières, N. Sangouard, M. Afzelius, H. de Riedmatten, and N. Gisin, Nature (London) **469**, 508 (2011).
[15] E. Saglamyurek, N. Sinclair, J. Jin, J. A. Slater, D. Oblak, F. Bussières, M. George, R. Ricken, W. Sohler, and W. Tittel, Nature (London) **469**, 512 (2011).
[16] M. Gündoğan, P. M. Ledingham, K. Kutluer, M. Mazzera, and H. de Riedmatten, Phys. Rev. Lett. **114**, 230501 (2015).
[17] A. Tiranov *et al.*, Phys. Rev. Lett. **117**, 240506 (2016).
[18] P. Jobez, N. Timoney, C. Laplane, J. Etesse, A. Ferrier, P. Goldner, N. Gisin, and M. Afzelius, Phys. Rev. A **93**, 032327 (2016).
[19] A. Seri, A. Lenhard, D. Rieländer, M. Gündoğan, P. M. Ledingham, M. Mazzera, and H. de Riedmatten, Phys. Rev. X **7**, 021028 (2017).
[20] K. Kutluer, M. Mazzera, and H. de Riedmatten, Phys. Rev. Lett. **118**, 210502 (2017).
[21] C. Laplane, P. Jobez, J. Etesse, N. Gisin, and M. Afzelius, Phys. Rev. Lett. **118**, 210501 (2017).
[22] T.-S. Yang *et al.*, Nat. Commun. **9**, 3407 (2018).
[23] S.-Y. Lan, A. G. Radnaev, O. A. Collins, D. N. Matsukevich, T. A. Kennedy, and A. Kuzmich, Opt. Express **17**, 13639 (2009).
[24] A. Nicolas, L. Veissier, L. Giner, E. Giacobino, D. Maxein, and J. Laurat, Nat. Photonics **8**, 234 (2014).
[25] D.-S. Ding, W. Zhang, Z.-Y. Zhou, S. Shi, G.-Y. Xiang, X.-S. Wang, Y.-K. Jiang, B.-S. Shi, and G.-C. Guo, Phys. Rev. Lett. **114**, 050502 (2015).
[26] Y.-F. Pu, N. Jiang, W. Chang, H.-X. Yang, C. Li, and L.-M. Duan, Nat. Commun. **8**, 15359 (2017).
[27] R. Chrapkiewicz, M. Dąbrowski, and W. Wasilewski, Phys. Rev. Lett. **118**, 063603 (2017).
[28] L. Tian, Z. Xu, L. Chen, W. Ge, H. Yuan, Y. Wen, S. Wang, S. Li, and H. Wang, Phys. Rev. Lett. **119**, 130505 (2017).
[29] N. Sinclair *et al.*, Phys. Rev. Lett. **113**, 053603 (2014).

[30] L. Olislager, J. Cussey, A. T. Nguyen, P. Emplit, S. Massar, J.-M. Merolla, and K. Phan Huy, Phys. Rev. A **82**, 013804 (2010).
[31] J. M. Lukens and P. Lougovski, Optica **4**, 8 (2017).
[32] D. Rielnder *et al.*, Quantum Sci. Technol. **3**, 014007 (2017).
[33] M. Kues *et al.*, Nature (London) **546**, 622 (2017).
[34] H.-H. Lu, J. M. Lukens, N. A. Peters, B. P. Williams, A. M. Weiner, and P. Lougovski, Optica **5**, 1455 (2018).
[35] E. Saglamyurek *et al.*, Nat. Commun. **7**, 11202 (2016).
[36] A. Seri, G. Corrielli, D. Lago-Rivera, A. Lenhard, H. de Riedmatten, R. Osellame, and M. Mazzera, Optica **5**, 934 (2018).
[37] D. Rieländer, K. Kutluer, P. M. Ledingham, M. Gündoğan, J. Fekete, M. Mazzera, and H. de Riedmatten, Phys. Rev. Lett. **112**, 040504 (2014).
[38] E. Pomarico, B. Sanguinetti, C. I. Osorio, H. Herrmann, and R. T. Thew, New J. Phys. **14**, 033008 (2012).
[39] See Supplemental Material at http://link.aps.org/supplemental/10.1103/PhysRevLett.123.080502 for further information on the frequency-multiplexed photon-pair source, on the storage protocol and its efficiency, on the analysis of the biphoton spectrum and on other small details.
[40] H. de Riedmatten, M. Afzelius, M. U. Staudt, C. Simon, and N. Gisin, Nature (London) **456**, 773 (2008).
[41] M. Afzelius, C. Simon, H. de Riedmatten, and N. Gisin, Phys. Rev. A **79**, 052329 (2009).
[42] P. Sekatski, N. Sangouard, F. Bussières, C. Clausen, N. Gisin, and H. Zbinden, J. Phys. B **45**, 124016 (2012).
[43] S. Fasel, O. Alibart, S. Tanzilli, P. Baldi, A. Beveratos, N. Gisin and H. Zbinden, New J. Phys. **6**, 163 (2004).
[44] J. Fekete, D. Rieländer, M. Cristiani, and H. de Riedmatten, Phys. Rev. Lett. **110**, 220502 (2013).
[45] A. Christ, K. Laiho, A. Eckstein, K. N. Cassemiro, and C. Silberhorn, New J. Phys. **13**, 033027 (2011).
[46] M. Grimau Puigibert, G. H. Aguilar, Q. Zhou, F. Marsili, M. D. Shaw, V. B. Verma, S. W. Nam, D. Oblak, and W. Tittel, Phys. Rev. Lett. **119**, 083601 (2017).
[47] M. Afzelius *et al.*, Phys. Rev. Lett. **104**, 040503 (2010).
[48] D. M. S. Johnson, J. M. Hogan, S. w. Chiow, and M. A. Kasevich, Opt. Lett. **35**, 745 (2010).
[49] A. Crespi, R. Osellame, R. Ramponi, M. Bentivegna, F. Flamini, N. Spagnolo, N. Viggianiello, L. Innocenti, P. Mataloni, and F. Sciarrino, Nat. Commun. **7**, 10469 (2016).
[50] Y. Chen, J. Gao, Z.-Q. Jiao, K. Sun, W.-G. Shen, L.-F. Qiao, H. Tang, X.-F. Lin, and X.-M. Jin, Phys. Rev. Lett. **121**, 233602 (2018).